IEEE Photonics Journal
An IEEE Photonics Society Publication

Open Access

Compact Polarization-Independent MMI-Based 1 × 2 Power Splitter Using Metal-Cap Silicon-on-Insulator Waveguide

Volume 8, Number 3, June 2016

Chao Pan
B. M. A. Rahman, Fellow, IEEE

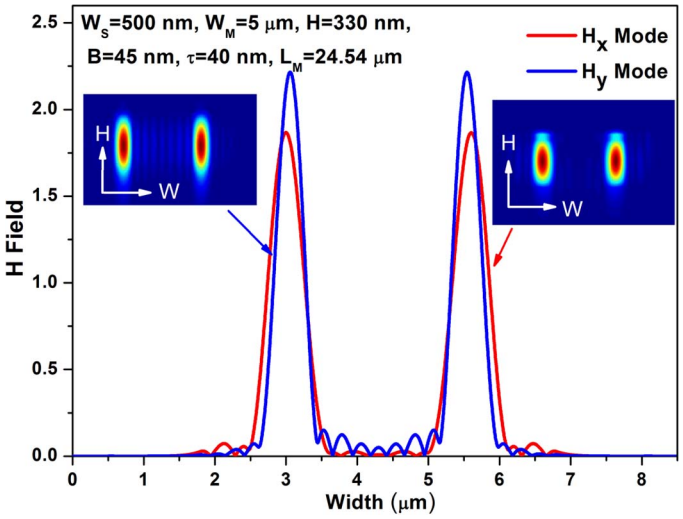

DOI: 10.1109/JPHOT.2016.2564926
1943-0655 © 2016 IEEE

IEEE photonics SOCIETY

IEEE

Compact Polarization-Independent MMI-Based 1 × 2 Power Splitter Using Metal-Cap Silicon-on-Insulator Waveguide

Chao Pan[1,2] **and B. M. A. Rahman,**[2] ***Fellow, IEEE***

[1]School of Electronic Science and Engineering, Southeast University, Nanjing 210096, China
[2]Department of Electrical and Electronic Engineering, City University London, London EC1V 0HB, U.K.

DOI: 10.1109/JPHOT.2016.2564926

Manuscript received April 15, 2016; accepted May 3, 2016. Date of publication May 9, 2016; date of current version May 18, 2016. Corresponding author: C. Pan (e-mail: P.C.1987@163.com).

Abstract: A compact polarization-independent multimode interference (MMI)-based 1 × 2 power splitter is designed by introducing a metal-cap silicon-on-insulator (SOI) waveguide as the MMI section, and its polarization and attenuation characteristics are optimized by using a full-vectorial **H**-field finite-element method (FEM). The least square boundary residual method is used to study the propagation process and the dependence of the image quality on the number of modes used. It is shown that a 330-nm-high, 5-μm-wide, and 24.54-μm-long MMI section can yield a polarization-independent 1 × 2 power splitter with the excess loss of only 0.66 and 0.86 dB for the quasi-transverse electric (TE) and quasi-transverse magnetic (TM) modes, respectively.

Index Terms: Polarization independent, multimode interference (MMI)-based power splitter, metal-cap silicon-on-insulator (SOI) waveguide, full vectorial H-field finite-element method (FEM).

1. Introduction

Power splitters and couplers are basic and important building blocks for photonic integrated circuits (PICs). Among all of the integrated optical implementations reported [1]–[3], the multimode interference (MMI) based power splitters have shown to have smaller foot print, better tolerance to fabrication errors, broader bandwidth, and lower polarization dependency for weakly restrictive waveguides. Strongly restrictive waveguides (WGs) based on silicon-on-insulator (SOI) which enables greater size reduction of PICs now is an area of major interest in photonics [4], but devices based on them are generally polarization dependent. However, design of polarization independent sub-systems or even a single component will provide additional flexibility [5]–[8]. It is true that polarization independent beam splitting of the two polarization waves in the bus nanowire is essential in the polarization multiplexing transmission system; otherwise, such a common system based on SOI platform can only support single point to single point communication. The length of a MMI-based power splitter depends on the beat length, L_π, which is related to the propagation constants of the first and second modes. Usually, effective indices (propagation constants) of transverse electric (TE) modes are larger than those of transverse magnetic (TM) modes, because width of the waveguide used is generally bigger than its height, especially for the MMI power splitter or coupler which requires bigger width to support enough higher order modes for high-quality interference image. The effective imaging distance for the

TE polarization is longer than that of the TM polarization, and thus, SOI MMI based power splitters are inherently polarization dependent. Earlier, an ultra-compact polarization-insensitive silicon-based strip-to-slot power splitter by using inverse-tapered subwavelength grating structure was reported [9], but this structure can be more complicated to fabricate. Thus, a compact polarization-insensitive MMI power splitter with low SOI thickness and easy to fabricate has yet to be reported.

Due to the surface plasmons (SP) effect, the effective indices of quasi-TM modes increase and those of quasi-TE modes decrease in the metal-cap (MC) SOI waveguide (WG) which contains a SiO_2 buffer layer between the metal cap and silicon core [10]. It is also observed in our work that the difference between the two lowest order quasi-TE modes increase a little, but that for TM mode decrease significantly, which provides an opportunity to design a polarization-independent MMI power splitter by adding a metal cap. A SiO_2 buffer layer is introduced to control the L_π ratio for TE and TM polarizations and also to reduce modal losses.

In this paper, design optimization of a compact polarization-independent MMI-based power splitter using a MC SOI WG is presented along with the study of the polarization and attenuation characteristics with the variations of the waveguide width and height of different layers by using a full vectorial **H**-field finite element method (FEM) in conjunction with the perturbation technique [11]. The length of MMI power splitter has a strong correlation with its width. Thus, in order to achieve a compact design, the influence of the number of the modes participating in forming the image, which is mainly determined by the WG width, on the quality of N-fold image is studied by the least-squares boundary residual (LSBR) method [12]. The excess loss of the device is comprised of the propagation loss of the MMI section due to the absorption in the metal cap and the coupling loss between the access SOI WGs and MMI section. The first one is obtained by the full vectorial **H**-field FEM in conjunction with the perturbation technique, while the second one is calculated by simulating the whole device by using the LSBR method.

2. Theory

The operation of an MMI-based device is based on the self-imaging principle [1]. The incident fundamental mode entering via the access waveguide will excite many higher order modes in the MMI region to satisfy the continuity of the input field. The propagation constants of these excited modes approximately follow, through a quadratic relationship given by [1]

$$\beta_0 - \beta_\nu = \frac{\nu(\nu+2)\pi}{3L_\pi} \tag{1}$$

where β_0 is the propagation constant of the fundamental mode in the MMI waveguide, ν is the mode number and L_π is the beat length of the two lowest order modes, and

$$L_\pi = \frac{\pi}{\beta_0 - \beta_1}. \tag{2}$$

If the quadratic relationship holds correctly, in the symmetric interference mechanism relating to an $1 \times N$ MMI power splitter whose input waveguide is placed to the center of the MMI section, N-fold image may be obtained at distance

$$L_N = \frac{1}{N}\frac{3L_\pi}{4} \tag{3}$$

by exciting only the even symmetric modes.

For a step-index multimode waveguide, L_π can also be approximated by the effective width W_e, which takes into account lateral penetration depth of the mode field

$$L_N = \frac{4n_r W_e^2}{3\lambda} \tag{4}$$

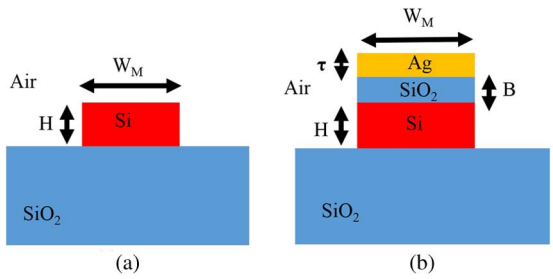

Fig. 1. (a) Diagram of a SOI WG. (b) Diagram of an MC SOI WG.

where n_r is the core (effective) refractive index of the waveguide, and λ is free-space wavelength. For simplicity, the effective width W_e can be approximated as [1]

$$W_e = W_M + \left(\frac{\lambda}{\pi}\right)\left(\frac{n_c}{n_r}\right)^{2\sigma}\frac{1}{\sqrt{n_r^2 - n_c^2}} \tag{5}$$

where $\sigma = 0$ for TE mode, $\sigma = 1$ for TM mode, W_M is the width of MM waveguide, and n_c is the cladding refractive index.

In the weakly restrictive waveguide, n_c is very close to n_r, and therefore, the value of n_c/n_r is nearly 1 and for quasi-TE and quasi-TM modes, the obtained L_π values are approximately equal. As a result, the MMI power splitter based on weakly restrictive waveguides are not polarization dependent. However, in the strongly restrictive waveguide such as the WG built on SOI platform shown in Fig. 1(a), the effective width W_e of the quasi-TE mode is broader than that of the quasi-TM mode, because n_r is significantly higher than n_c and σ for TM mode is larger than that for TE mode. Besides that, it should be noted that for SOI WG with SiO_2 substrate and air cladding, the boundary condition of the bottom interface of WG is different from the others, and therefore, (5) can only be used as an approximation. The L_π values of different polarization modes will show relatively larger difference according to (4). Thus, the splitter is relatively sensitive to polarization in a strongly restrictive SOI WG.

Because of the SP effect, the metal cap of the MC SOI WG which may contain a SiO_2 buffer between silicon core and the metal cap, as shown in Fig. 1(b), is expected to demonstrate its influence on the field distribution of the TM modes when the SiO_2 buffer is very thin. Compared with the field distributions of the TM modes in the SOI WG, more field will be confined in the core and SiO_2 buffer due to the boundary condition of the vertical electrical field. Besides, in order to avoid the field being mainly confined in the low index SiO_2 buffer layer, as in a plasmonic slot waveguide, the height of the silicon core, H should be large enough. Therefore, the effective width W_e may increase, and its effective index will become larger. On the other hand, the field distributions of TE modes in the MC SOI WG whose electrical field is horizontal will remain similar to that in SOI WG. Based on this principle, the L_π values of the TE and TM modes in the MC SOI WG may be made equal to each other by adjusting various parameters of the waveguide, and thus the design of a polarization-independent MMI power splitter may be achieved based on employing metal-cap waveguide as the MMI section. On the other hand, the propagation loss of the MC SOI WG will be bigger than that of the SOI WG because part of the field power will be absorbed by the metal cap. Even worse, apparently, the loss of the MC SOI WG will increase when the thickness of the SiO_2 layer becomes thinner. This phenomena may bring a limitation to realize a practical MMI power splitter based on the MC SOI WG, and thus, the loss values are also required to be studied.

It can be noted that (4) and (5) are not suitable to obtain the L_π values of TE and TM modes in the MC SOI WG whose structure is not simple. Therefore, an accurate numerical approach is needed to obtain the L_π values of different polarization modes. On the other hand, as for all practical optical waveguide with 2-D confinement, the eigenmodes are classified as quasi-TE and quasi-TM modes, and they contains all the six components of **E** and **H** fields. In this case, a

Full vectorial **H**-field based finite element method [13], which is one of the most accurate and numerically efficient approaches, is used to find eigenmodes here.

As the MC SOI WG contains a layer of metal cap with complex refractive index, modal loss is introduced. However, most of the formulations used in FEM, such as and **H**-field formulation [13] given above, are restricted to structures without modal loss or gain. The loss/gain factor can be calculated by solving complex eigenvalue equations associated with the scalar [14], and vector E_Z/H_Z [15], H_t [16] and **H**-field [17] formulations. For most practical waveguides, loss or gain values could be limited, and the imaginary part of the complex propagation constant is small compared to the real part. The full-vectorial **H**-field formulations in conjunction with the perturbation technique [11] is a more suitable approach to calculate the modal loss values for such waveguides. When using the FEM, the field distribution in the transverse plane is obtained by the application of the variational formulation. The usual time and axial dependencies are given by $\exp(j\omega t)$ and $\exp(-\gamma z)$, respectively, for angular frequency ω and time t, where $\gamma = \alpha + j\beta$ is the complex propagation constant in the z direction, and β and α are the phase and attenuation constants, respectively. The perturbed fields are approximated by the fields obtained from the solution of variational formulation, using only the real part of the dielectric constant. The attenuation constant is then calculated from the results from the loss-free system by using simple matrix multiplication [11]. This approach may reduce the slow calculation time and large memory required in other formulations, such as the H_t formulation.

The beam propagation method (BPM) [18] is a useful approach to study the evolution of optical waves along z-variant optical structures and calculate the power transfer during modal conversion. However, for the MMI power splitter composed of three sections of straight waveguides with only two simple junctions, a junction analysis approach would be numerically more efficient. The least-squares boundary residual (LSBR) method is more accurate than the other available techniques for the analysis of power transfer characteristics in practical guided-wave problems [19]. The LSBR method looks for stationary solution to satisfy the continuity conditions of the tangential **E** and **H** fields in a least squares sense over the interface by minimizing the error energy functional, J, as given [12]

$$J = \int \left|E_t^I - E_t^{II}\right|^2 + a \cdot Z_0^2 \left|H_t^I - H_t^{II}\right|^2 d\Omega \tag{6}$$

where Z_0 is the free-space wave impedance, and a is the dimensionless weighting factor to balance the electric and magnetic components of the error functional. The integration is carried out over the junction interface, Ω, between the access and asymmetric Silicon nanowires. For the structure with one or two junctions, this method would be more efficient and rigorous than the BPM. Besides that, the least required number of the modes for the MMI device can also be identified by changing the number of the modes used in the LSBR method. Thus, the width and length of MMI section can be optimized to achieve a compact yet satisfactory design.

3. Results

First, the effect of the metal cap to the real part of the effective index, n_{eff} is tested by comparing the variations of the effective indices of eigenmodes including the fundamental quasi-TE, H_y^{11}, and quasi-TM, H_x^{11} modes, and the first higher order quasi-TE, H_y^{21}, and quasi-TM, H_x^{21} modes with the widths of the SOI WG and the MC SOI WG shown in Fig. 2. The SOI WG here is cladded by air. The height of the silicon core for both the WGs is taken as 220 nm. The thicknesses of SiO_2 buffer and metal cap of the MC SOI WG are initially taken as 75 nm and 45 nm, respectively, and later on these are optimized. The refractive indices of Silicon and Silica are taken as 3.475 and 1.444 at the operating wavelength of 1550 nm, respectively. The relative permittivity of the metal cap, silver is taken as $-129.17 + j3.2841$. Effective indices for the SOI WG and MC SOI WG are shown by blue and red lines, respectively. It is obvious that both kinds of WGs have some characteristics in common: 1) The effective indices of the all the quasi-TE and quasi-TM modes increase rapidly at first and then reach their stable values asymptotically when the WG

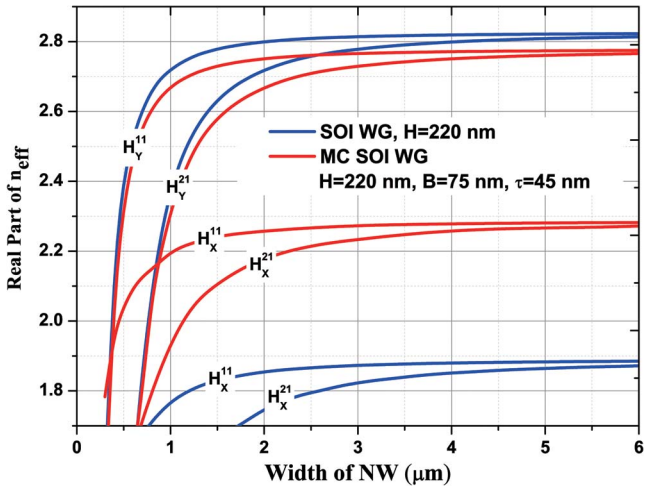

Fig. 2. Variations of the effective indices of the eigenmodes with the WG width for the SOI WG and MC SOI WG.

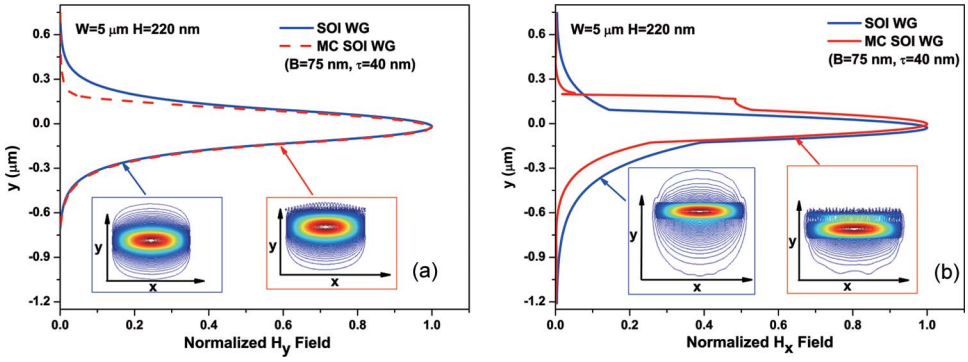

Fig. 3. (a) Normalized H_y field of the H_y^{11} modes in the SOI WG and MC SOI WG. (b) Normalized H_x field of the H_x^{11} modes in the SOI WG and MC SOI WG.

width increases; and 2) the effective index of the quasi-TE mode is bigger than that of the quasi-TM mode with the same mode order when the WG width is big enough. It can be observed that the effective indices of all the quasi-TE modes in the MC SOI WG are slightly less than those of all the quasi-TE modes in the same SOI WG. However, for all the quasi-TM modes, their indices in the MC SOI WG are significantly larger than those in the same wide SOI WG.

Ideal metal wall forces $n \cdot H = 0$, which makes $H_y = 0$ at the horizontal metal interface. Neumann boundary condition is introduced for H_x. Thus an ideal metal cap introduce a mirror with symmetry for quasi-TM mode, with dominant H_x field, which mimics even coupled supermode and n_{eff} increases. On the other hand, the Dirichlet boundary condition on a dominant H_y field mimics the antisymmetry mirror for the quasi-TE mode, and as a result, n_{eff} reduces, similar to an odd supermode. This has been verified in Fig. 2, but a real metal layer is represented here by its complex refractive index, and as a result the value of n_{eff} is also complex whose real part indicates the phase propagation, and imaginary part indicates the attenuation of the power. The 2-D H_y field contours of the fundamental quasi-TE, H_y^{11} modes in the two WGs with the same width and silicon core height are given as the insets in Fig. 3(a), while the 2-D H_x field contours of the fundamental quasi-TM, H_x^{11} modes in the two WGs are given as the insets in Fig. 3(b). It can be observed that the H_y field contours of the H_y^{11} mode in MC SOI WG near metal cap is restricted at the interface between the metal cap and air, and the H_x field of the H_x^{11} mode in the MC SOI WG

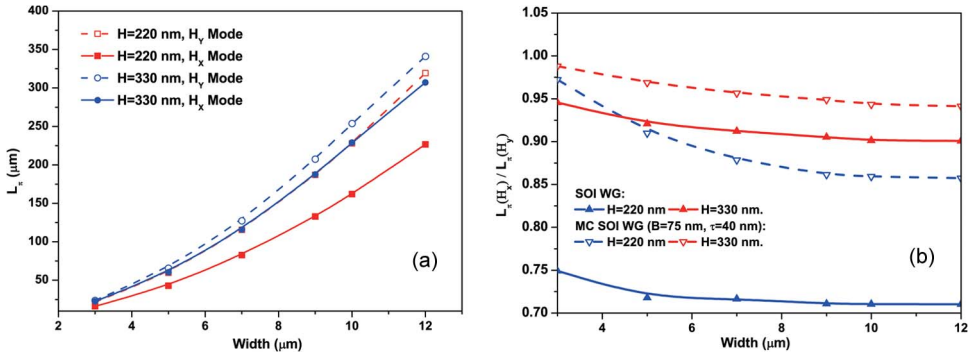

Fig. 4. (a) Variations of the beat lengths of the H_x and H_y modes in the SOI WG with its width for two different heights. (b) Variations of the ratio of the beat lengths of the H_x and H_y modes in the SOI WG and MC SOI WG with their widths for three different heights.

is mainly distributed in silicon core and SiO_2 buffer due to SP effect, and it is also restricted at the interface between the metal cap and air. In order to show the difference of the magnitude of the field in the two WGs clearly, the field profiles at the center of the WGs along *y*-direction (height-direction) are shown in Fig. 3. It is clear that the distributions of H_y field of the H_y^{11} modes in the silicon cores of SOI WG (shown by a blue solid line) and MC SOI WG (shown by a red dashed line) are almost the similar except lower field value at the metal interface for MC SOI WG. On the other hand, the H_x field profile of the H_x^{11} mode in the MC SOI WG [shown by a red solid line in Fig. 3(b)] increases at the metal interface and plasmonic peaks are clearly visible at the two metal interfaces. When a metal cladding layer is introduced, more fields are confined in the silicon core for the quasi-TM modes due to the plasmonics effect, resulting for their effective indices to increase. This also reduces the difference between β_0 and β_1, and as a result its L_π will increase and can bring the imaging distances for quasi-TE and quasi-TM modes closer and reduce their polarization dependence.

After verifying the effect of the metal cap on the effective indices and the field distributions in the MC SOI WG, we calculated the beat lengths of the quasi-TE, H_y and quasi-TM, H_x modes for different widths and heights of the silicon cores in the WGs. Here, instead of using the approximate (4), the beat length is calculated via (2) after the propagation constants of the fundamental and the first higher order modes are accurately calculated by the full-vectorial FEM. The variations of the beat lengths of the H_y and H_x modes in the SOI WG with its width for heights of 220 nm and 330 nm are shown in Fig. 4(a) by red dashed and solid lines and blue dashed and solid lines, respectively. It is obvious that the beat lengths of both the H_y and H_x modes will increase strongly with the increase in the WG width, which agrees with the trend implied by (4); therefore, the width of the MMI section for MMI power splitter should be narrow enough to reach a compact design, but also wide enough to obtain a good interference image. The beat lengths of both the H_y and H_x modes will increase slightly with the increase in the WG height as modes get more confined and the difference between the propagation constants of the fundamental and higher order modes, $\Delta\beta$ reduces. It also shows that the L_π value for the H_x modes is smaller than that for the H_y modes, as the H_y modes are more confined (their n_{eff} are higher and $\Delta\beta$ are smaller), which is also supported by (5) as lower σ for the H_y modes makes W_e larger. However, the difference between the H_y and H_x modes reduces with the increase of the height. The beat lengths of the H_y and H_x modes in the MC SOI WG with different dimensions are also calculated but now shown here. It was observed that the beat length of H_x mode increases significantly when employing the metal cap to the SOI WG, especially for the WGs with lower height. However, as to the H_y mode, the beat length only decreases a little. For instance, when the width and height of the SOI WG are taken as 3 μm and 220 nm, respectively, the beat length of H_x mode will be increased from 16.198 to 20.607 μm after adding a 75 nm-thick buffer layer and 45 nm-thick metal cap, but for H_y mode, it decreased only by ~ 0.5 μm.

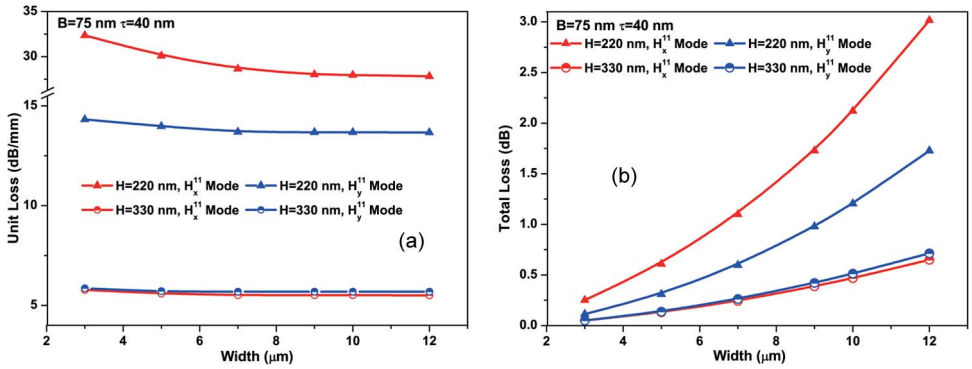

Fig. 5. Variations of (a) the unit loss of the MC SOI WG and (b) the total loss of the MMI section based on it for MMI-based 1 × 2 power splitter for the H_x^{11} and H_y^{11} modes with its width for different heights.

The key parameter for designing a polarization-independent MMI power splitter is the L_π ratio for two polarizations. Variations of the ratio of the beat lengths of the H_x and H_y modes, $L_\pi(H_x)/L_\pi(H_y)$ in the SOI WG with their widths for heights of 220 nm and 330 nm are plotted by solid blue and red lines, respectively in Fig. 4(b). These ratios for MC SOI WG are shown by dashed blue and red lines for $H = 220$ nm and 330 nm, respectively. Here, a fixed metal thickness $\tau = 40$ nm and SiO_2 buffer thickness $B = 75$ nm are considered but later on effect of these layer thicknesses are also considered. It can be observed that all the ratios for both the metal-cap and uncapped WGs will decrease slowly with the increase in their widths at first and then reach stable values for all heights considered here. It can also be observed that when adding a metal cap to SOI WG, the ratios will rise, and the effect is more obvious when the silicon core height is lower. As to the smaller height, field is less confined vertically, more expanded, so more strongly influenced by the presence of the metal wall. For example, when the width of the WG is taken as 5 μm, after adding the metal cap, the ratios are increased from 0.718 to 0.910 and from 0.921 to 0.969 for $H = 220$ nm and $H = 330$ nm, respectively.

However, resulting propagation loss of the MC SOI WG is much larger than that of the SOI WG due to the additional absorption in the metal cap. Variations of the unit loss (dB/mm) of the MC SOI WG for the H_x^{11} and H_y^{11} modes with its width for different heights are shown in Fig. 5(a) by using blue and red lines, respectively. It can be observed that all the unit loss decreases at first and then reach a stable value with the increase in the width, and increases strongly with the decrease in the height, especially for the H_x^{11} mode. For a thinner Si layer, mode is less confined in the core, more fields exist at the metal interface, and thus, modal loss increases. It can also be observed that for the waveguide with the height of 220 nm, the unit loss of H_x^{11} mode is almost twice bigger than that of H_y^{11} mode, and for the waveguide with the height of 330 nm, the unit loss of H_x^{11} mode is almost similar as the H_y^{11} mode. This phenomena is caused by the characteristic of **E** and **H** field distribution in a 2-D confined waveguide. It is well known that quasi-TM mode with dominant H_x field is strongly affected by the presence of a horizontal metal layer. On the other hand, quasi-TE mode with its dominant H_y field is less influenced by such a metal layer. However, for a silicon NW with strong index contrast, its quasi-TE mode can have a higher value of its non-dominant H_x field and such a field located at the upper silicon interface can be affected by the presence of a closely located metal layer.

The loss of the MMI section is defined as the total loss, when MC SOI WG is employed as the MMI section for a MMI-based 1 × 2 power splitter. However, scattering loss is ignored here, but if needed this can also be included. Variations of the total loss (dB) with the width are shown in Fig. 5(b). As the unit loss changes only slightly with the change of the WG width, but the quadratic increase of the beat length with the WG width, which was shown in Fig. 4(a), will mainly contribute to the increase of total loss of the MC SOI WG with its width as shown here.

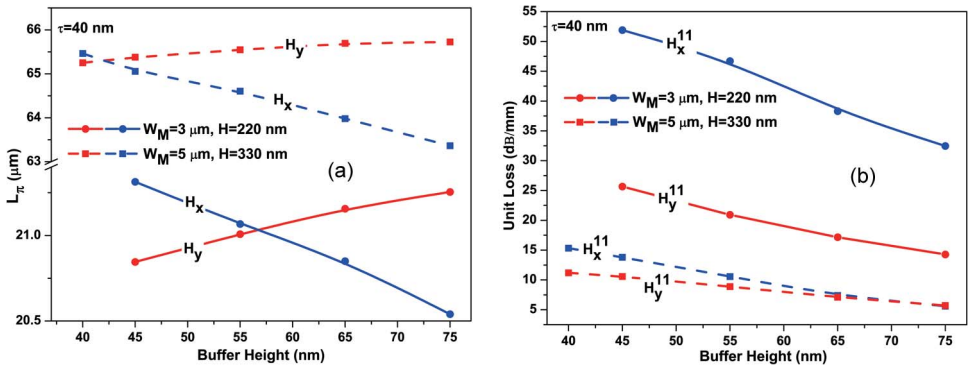

Fig. 6. Variations of (a) the beat lengths of the H_x and H_y modes and (b) the unit loss of the H_x^{11} and H_y^{11} modes in the MC SOI WG with the height of SiO_2 buffer for two different WG dimensions.

According to (3), the length of the MMI section here is set to $3L_\pi/8$ for 1×2 splitter with $N = 2$. The total loss of the H_x^{11} and H_y^{11} modes passing through the MMI section with the silicon core height of 220 nm and the width of 3 μm is about 0.25 dB and 0.114 dB, respectively, while for the WG with the silicon core height of 330 nm and the width of 5 μm, it is about 0.13 dB and 0.137 dB, respectively.

The above result shows that although the modal loss exists, however, it is relatively small and may be acceptable when the beat lengths of the H_x and H_y modes in the MC SOI WG are made equal for its polarization independent operation. As both the plasmonic metal loss and the beat length ratio of two polarizations depend on the buffer layer thickness, next, the height of the SiO_2 buffer is varied to study this. Variations of the beat lengths, L_π of the H_x and H_y modes in the MC SOI WG for the widths of 3 μm and 5 μm are shown in Fig. 6(a) by red and blue solid, and red and blue dashed lines, respectively. The heights of the silicon core for 3 μm- and 5 μm-width cases are taken as 220 nm and 330 nm, respectively. The thickness of the metal cap for the both cases is taken as 40 nm. It can be observed that with the increase in the buffer height, the beat length for the H_x modes slightly decreases, while that for the H_y modes slightly increases. It should be noted that such a variation is small, less than 2 μm when the buffer height increases from 45 nm to 75 nm. It is clear from these studies that the beat lengths of the two polarization modes can be made equal at a specific value of the SiO_2 buffer height. For the waveguides with $W_M = 3$ μm and $H = 220$ nm, and $W_M = 5$ μm and $H = 330$ nm, the heights of SiO_2 buffer are 56 nm and 42 nm, respectively, when the ratio can be made equal to 1. Fig. 6(b) shows the variations of the unit loss of the H_x^{11} and H_y^{11} modes in the MC SOI WG with the buffer height for the waveguides with the two different dimensions. It can be clearly observed that the unit loss decreases with the increase of the buffer height. Because the beat length does not change significantly with the variation of the buffer height, the total loss of the MC SOI WG used as the MMI section for a MMI-based 1×2 power splitter have a similar tendency as the unit loss. The total loss of the H_x^{11} and H_y^{11} modes in the WG with the width of 3 μm, the silicon core height of 220 nm, the buffer height of 55 nm, and the metal cap thickness of 40 nm is 0.364 dB and 0.165 dB, respectively, while that of the H_x^{11} and H_y^{11} modes in the WG with the width of 5 μm, the silicon core height of 330 nm, the buffer height of 45 nm, and the metal cap thickness of 40 nm is 0.337 dB and 0.259 dB, respectively.

Next, the influence of the metal cap thickness is studied. Variations of the beat lengths of the H_x and H_y modes in the MC SOI WG with the metal cap thickness for two different WG dimensions are shown in Fig. 7(a). For one set, the heights of the silicon core and the SiO_2 buffer are 220 nm and 55 nm, respectively, when the width of the waveguide is 3 μm. For the other WG with the width of 5 μm, the heights of the silicon core and the SiO_2 buffer are 330 nm and 45 nm, respectively. It can be observed that with the increase in the metal cap thickness, the beat length for the H_x modes decreases only slightly, while that for the H_y modes remains very

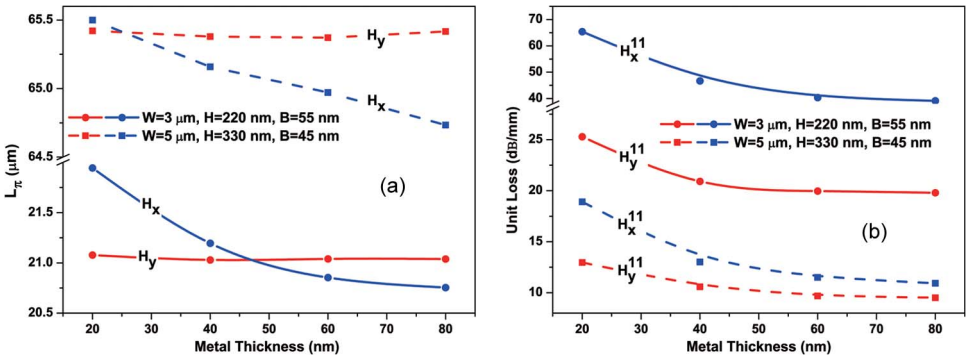

Fig. 7. Variations of (a) the beat lengths of the H_x and H_y modes and (b) the unit loss of the H_x^{11} and H_y^{11} modes in the MC SOI WG with the thickness of MC for two different WG dimensions.

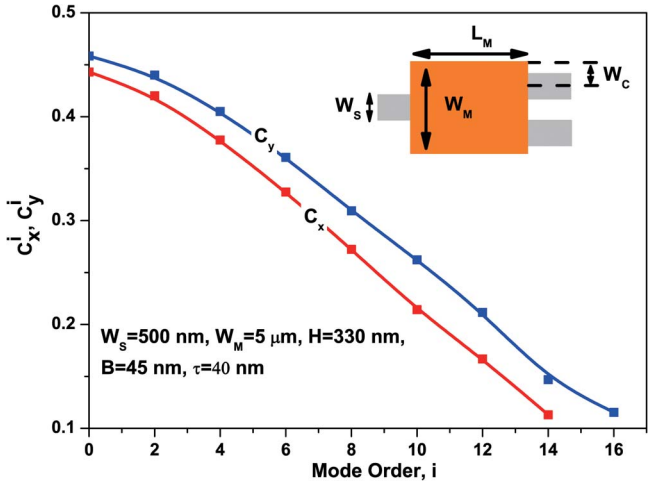

Fig. 8. Variations of the transmitted modal coefficients C_x^i and C_y^i with the order i of the even modes exiting in the MC SOI WG.

almost constant. It can also be observed that the ratio of the beat lengths for the H_x and H_y modes can also be adjusted to 1 by changing the metal cap thickness for these two cases. Variations of the unit loss of the H_x^{11} and H_y^{11} modes in the MC SOI WG with the metal cap thickness for the two WGs are shown in Fig. 7(b). It is shown here that in all the cases, the unit loss decreases at first and then becomes saturated when the metal cap thickness increases, and the unit loss of the H_x^{11} mode is significantly bigger than that of the H_y^{11} mode because the heights of silicon core and SiO_2 buffer are smaller in these two cases.

After optimizing the parameters of the MC SOI WG employed as the MMI section for the polarization-independent MMI-based 1 $\times$ 2 power splitter, the LSBR method is applied to calculate the power transmission between the access SOI WGs and the MMI section, and the evolution of the interference image in the MMI section. For the input SOI WG is placed to the center of the MMI section as shown in the Fig. 8, only the even modes in the MMI section are excited following the symmetric interference mechanism. The approach yields the transmitted modal coefficients of the even modes in the MMI section to satisfy the continuity of the tangential Electric and Magnetic fields. The MMI section with the width of 5 μm, the silicon core height of 330 nm, the SiO_2 buffer height of 45 nm, and the metal cap thickness of 40 nm is taken for evaluation. The access SOI WG for this case is 500 nm wide, and 330 nm high. Variations of the transmitted modal coefficients, C_x^i for the ith order even H_x modes in the MMI section excited by the fundamental quasi-TM mode, H_x^{11} in the input WG, and the transmitted modal coefficients, C_y^i

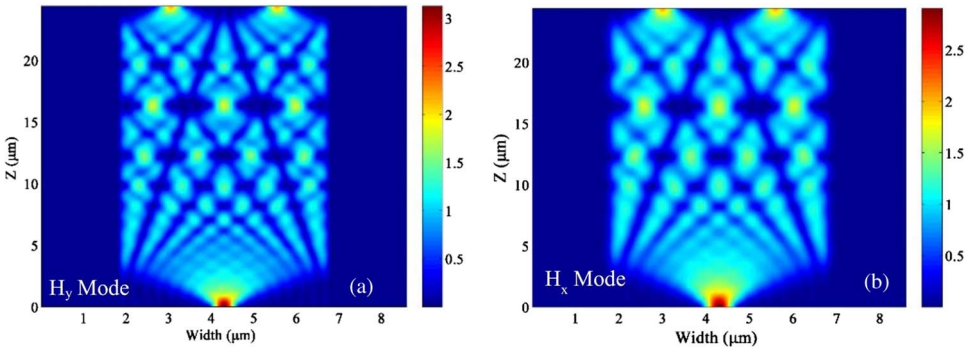

Fig. 9. Field distribution along the z-direction in the MMI section for the MMI-based 1 $\times$ 2 power splitter. (a) H_y field distribution of the H_y mode. (b) H_x field distribution of the H_x mode.

for the ith order even H_y mode in the MMI section excited by the fundamental quasi-TE mode, H_y^{11} in the input WG with their order, i, are shown by red and blue lines, respectively, in Fig. 8. It is shown that the modal coefficients decrease with the increase of the mode order, and C_y^i is slightly bigger than C_x^i for the same order, i.

After obtaining the all the transmitted modal coefficients by using the LSBR method, we simulated the interference image in the MMI section along the z-direction (propagation direction) for this case. Fig. 9(a) and (b) give the field distribution of the H_y and H_x modes along z-direction at the center (vertical) of MMI section, respectively. The waveguide can support nine even H_y modes and eight even H_x guided modes. It is clear that the high-quality image can meet the requirement of a 1 $\times$ 2 power splitter.

According to Eq. (3), for the MMI section with the width of 5 μm, silicon core height of 330 nm, buffer height of 45 nm, and metal cap thickness of 40 nm, its length for 1 $\times$ 2 power splitters is 24.50 μm and 24.58 μm for the H_x and H_y modes, respectively, which is very close. The H_x field contours of the H_x mode and the H_y field contours of the H_y mode on the output transverse face of MMI section with length of 24.54 μm are given as insets in Fig. 10(a). In order to show the magnitude of the field clearly, the dominant component of the **H** field at the center of the output transverse face of the MMI section along x-direction (width-direction) for the H_x and H_y modes are shown by red and blue lines, respectively. It can be observed that the widths of the H_x field of the H_x mode and the H_y field of the H_y mode on the output transverse face of the MMI section are nearly the same, and the polarization-independent MMI-based 1 $\times$ 2 power splitter can be realized based on the MMI section proposed here, which is composed of the single straight MC SOI WG. The excess loss of the whole device is comprised of the propagation loss of MMI section due to the absorption of the metal cap and the coupling loss between access SOI WGs and MMI section. Setting the distance between the center of one of the output SOI WGs and the close edge of MMI section, W_C to 1.2 μm (see Fig. 8), the total coupling loss between the access air-clad SOI WGs and the MMI section for the H_y and H_x modes is about 0.40 dB and 0.60 dB, respectively, calculated by the LSBR method. Adding the metal loss of the MMI section, the excess loss of the polarization-independent MMI-based 1 $\times$ 2 power splitter is about 0.66 dB and 0.86 dB for the H_y and H_x modes, respectively. However, instead of air-clad SOI WG as access waveguide, if a silica-clad SOI WG is used as the access waveguide then the total loss would be reduced by 0.1 dB due to a better field matching for both the quasi-TE and quasi-TM modes across the junctions. The larger coupling loss for the H_x mode than that for the H_y mode is due to larger mode-size mismatch between the SOI WG and the MC SOI WG for the H_x mode, which can be observed in Fig. 3. Although a good 2-fold interference image can be obtained in the 3 μm-wide MC SOI WG with the silicon core height of 220 nm, for the H_x mode, the mode-size mismatch between the SOI WG and the MC SOI WG becomes extremely serious, and the coupling loss for each interface is as large as 0.97 dB.

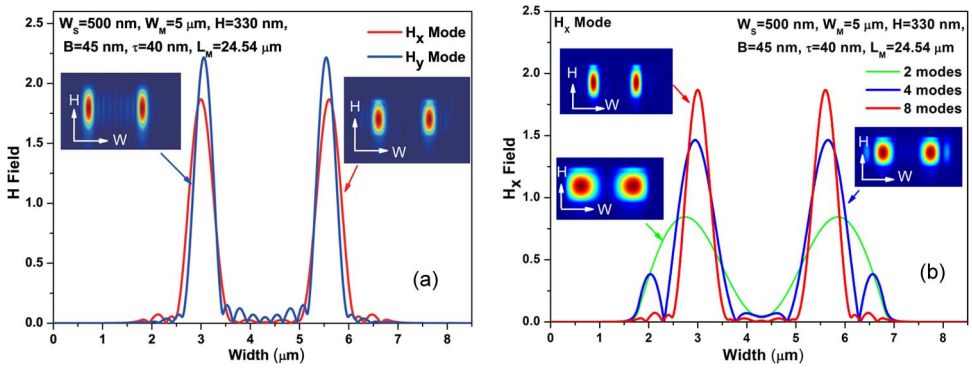

Fig. 10. (a) H_x field of the H_x mode and H_y field of the H_y mode on the output transverse face of the MMI section for the MMI-based 1 $\times$ 2 power splitter. (b) H_x field on the output transverse face of the MMI section for the MMI-based 1 $\times$ 2 power splitter for different numbers of even modes participating in forming the image.

The influence of the number of the excited even modes used for interference to the quality of the image is also tested by LSBR method. This approach allows us to include or exclude excited modes to see their effects on the image quality. However, in a physical system, it is not possible to include or exclude modes as we wish, but the mode number excited can be controlled by adjusting the width of the MMI section. The H_x field contours on the output interface of the MMI section for the polarization-independent MMI-based 1 $\times$ 2 power splitter for different numbers of the even modes participating in the forming the image are shown as separate insets in Fig. 10(b). The length of the MMI section is set to 24.54 μm. For only 2 even modes case, only the fundamental and the second higher order quasi-TM, H_x^{11}, H_x^{31} modes are used. For the 4 even modes case, the following fourth, and sixth higher order quasi-TM, H_x^{51}, H_x^{71}, modes are added. For the 8 even modes case, all eight even modes are used. In order to show the magnitude of the field clearly, the field at the center of the output transverse face of the MMI section along *x*-direction (width-direction) for 2, 4, and 8 even modes cases are also shown by green, blue, and red lines, respectively, in Fig. 10(b). It can be observed that the interference based on the higher number of even modes can provide higher-quality image. As we know that image quality depends on the number of modes in forming the image, while a better image quality can be obtained by using a wider MMI section, but consequently the device length will also increase.

Based on this, the width of the MMI section is decreased to 3 μm, while its silicon core height is kept unchanged to test the image quality. The SiO_2 buffer height and the metal cap thickness are set to 70 nm and 40 nm, respectively, to ensure the ratio of the beat lengths for the H_x and H_y modes to be 1 for this case. Only five even H_x and H_y modes exist in the 3 μm-wide WG. The width of the input access SOI WG is 400 nm. The H_y fields at the center of the output transverse face for the MMI section based on the MC SOI WG along x-direction (width-direction) for the two cases with different widths are compared. As the field is symmetric, only half part of the field is shown for comparison, and the center of the half part of the field for both cases is moved to zero point of x axis (width axis), shown in Fig. 11. It is obvious that the sidelobe of the field for the case with the width of 3 μm is significantly bigger than that for the case with the width of 5 μm. Besides that, the width of the main lobe for the narrow width case broadens which is expected to be 400 nm. Thus, wider output SOI WGs should be used for coupling at the output interface of MMI section. The width of the output WGs used here are 500 nm. The total coupling loss for all the input and output interfaces between the access SOI WGs and the MMI section for the H_y and H_x modes is about 0.70 dB and 0.80 dB, respectively. The total loss of the MMI section for the H_y and H_x modes is about 0.12 dB and 0.26 dB, respectively. In comparison with the case of the wider width, for the narrow 3 μm-wide design, the excess loss for the H_y and H_x modes are increased to 0.82 dB and 1.06 dB, besides slightly poorer image formation, although the length of MMI section can be significantly reduced from 24.54 μm to only 8.86 μm.

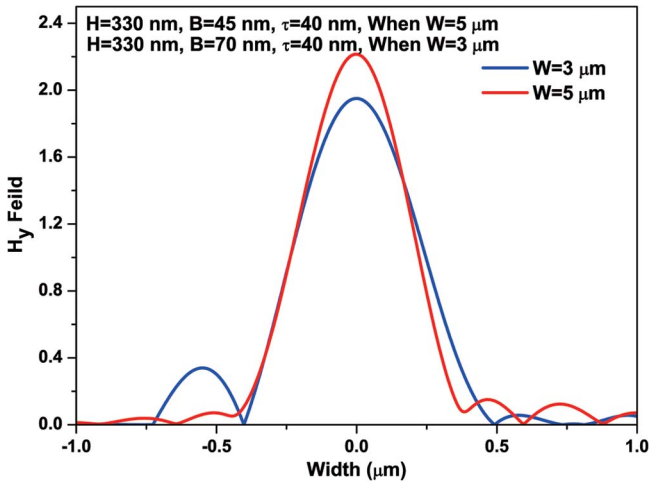

Fig. 11. Half part of the H_y field on the output transverse face of the MMI section along the width direction for the MMI sections with the two dimensions.

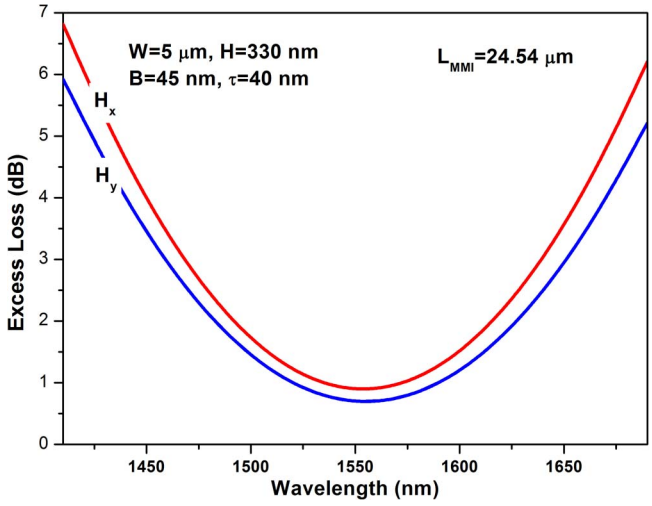

Fig. 12. Variations of the excess loss of the MMI power splitter based on the MC SOI WG for the H_y and H_y modes with the operating wavelength.

It is well known that traditional MMI-based power splitters have better tolerance to fabrication errors. As to MMI section based on MC SOI NW, Figs. 5 and 6 show that it is not sensitive to the small change of its width. It can be observed from Fig. 7 that the device is slightly sensitive to change of buffer layer height. The ratio of the beat length for H_x and H_y modes and the total loss of the MMI section will be changed only by ~2% and ~0.15 dB, for ±10 nm fabrication error, respectively. However, it can also be observed from Fig. 8 that the change of the ratio is less than 1% and that the change of the total loss is less than 0.1 dB when the metal cap thickness is changed by 10 nm.

Next, wavelength dependence of this power splitter is studied. Variations of the excess loss with the operating wavelength are shown in Fig. 12 for both the polarizations. It is well known that, as the wavelength is increased, modes become weakly confined, and as a result, the L_π (and the required device length) reduces. Any deviation of the L_π from the $L_{\pi 0}$ (at design wavelength of 1550 nm) will deteriorate the image. This will also reduce the power coupled to the two output ports. It can be observed in Fig. 12 that as wavelength deviates from the design

wavelength of 1550 nm, power loss increases. However, the excess loss in the range of 1500 nm to 1600 nm operating wavelength can be negligible.

4. Conclusion

The design of a compact polarization-independent MMI-based 1 $\times$ 2 power splitter is realized successfully by employing the MC SOI WG, which contains three layers: silicon core, SiO_2 buffer, and metal cap, as the MMI section. The width and the height of each layer are optimized to make the ratio of the beat lengths for the H_x and H_y modes in the WG to be 1 with low propagation loss by using the FEM and perturbation technique. The total propagation loss of the 5 μm-wide MMI section with 330 nm-high core is about 0.259 dB and 0.337 dB for the quasi-TE and quasi-TM modes, respectively. The coupling loss between access SOI WG and the MMI section caused by the mode-size mismatch which exists at the interfaces between two different kinds of WGs, together with the interference image in MMI section is calculated by the LSBR method. It is shown here that higher silicon height such as 330 nm would be preferable for the design with low loss. The excess loss of the 1 $\times$ 2 power splitter based on the MMI section with the width of 5 μm, silicon core height of 330 nm, SiO_2 buffer height of 45 nm, metal cap thickness of 40 nm, and length of 24.54 μm is about 0.66 dB and 0.86 dB for the H_y and H_x modes, respectively. Due to the mechanism of the LSBR method, the least number of the modes required for a good interference image is also studied, which can help to minimize the dimension of the MMI section. The length of the MMI section can also be reduced to 8.86 μm by decreasing its width to 3 μm, but the image quality will deteriorate and the excess loss will slightly increase to about 0.82 dB and 1.06 dB for the H_y and H_x modes, respectively, which may be reduced by the optimization of the access WG such as using tapered or SiO_2-cap structure.

References

[1] L. B. Soldano and E. C. M. Pennings, "Optical multi-mode interference devices based on self-imaging: Principles and applications," *J. Lightw. Technol.*, vol. 13, no. 4, pp. 615–627, Apr. 1995.

[2] H. Li, X. Dong, Z. L. E. Li, and Y. Bai, "Design optimization and comparative analysis of silicon-nanowire-based couplers," *IEEE Photon. J.*, vol. 4, no. 5, pp. 2017–2026, Oct. 2012.

[3] P. E. Morrissey, H. Yang, R. N. Sheehan, B. Corbett, and F. H. Peters, "Design and fabrication tolerance analysis of multimode interference couplers," *Opt. Commun.*, vol. 340, pp. 26–32, Nov. 2014.

[4] R. Soref, "Silicon photonics: A review of recent literature," *Silicon*, vol. 2, no. 1, pp. 1–6, Feb. 2010.

[5] P. Dong, Y. K. Chen, G. H. Duan, and D. T. Neilson, "Silicon photonic devices and integrated circuits," *Nanophoton.*, vol. 3, no. 4/5, pp. 215–228, Aug. 2014.

[6] Y. Qin *et al.,* "Silicon based polarization insensitive filter for WDM-PDM signal processing," *Opt. Exp.*, vol. 21, no. 22, pp. 25727–25733, Oct. 2013.

[7] D. Dai, Y. Shi, and S. He, "Theoretical investigation for reducing polarization-sensitivity in si-nanowire-based arrayed-waveguide grating (de)multiplexer with polarization-beam-splitters and reflectors," *IEEE J. Quantum Electron.*, vol. 45, no. 6, p. 654–660, Jun. 2009.

[8] D. X. Xu, S. Janz, and P. Cheben, "Design of polarization-insensitive ring resonators in silicon-on-insulator using MMI couplers and cladding stress engineering," *IEEE Photon. Technol. Lett.*, vol. 18, no. 2, pp. 343–345, Jan. 2006.

[9] Y. Xu and J. Xiao, "An ultracompact polarization-insensitive silicon-based strip-to-slot power splitter," *IEEE Photon. Technol. Lett.*, vol. 28, no. 4, pp. 536–539, Feb. 2016.

[10] D. Dai and S. He, "A silicon-based hybrid plasmonic waveguide with a metal cap for a nano-scale light confinement," *Opt. Exp.*, vol. 17, no. 19, pp. 16646–16653, Sep. 2009.

[11] C. Themistos, B. M. A. Rahman, A. Hadjicharalambous, and K. T. V. Grattan, "Loss/gain characterization of optical waveguides," *J. Lightw. Technol.*, vol. 13, no. 1, pp. 1760–1765, Aug. 1995.

[12] B. M. A. Rahman and J. B. Davies, "Analyses of optical waveguide discontinuities," *J. Lightw. Technol.*, vol. 6, no. 1, pp. 52–57, Jan. 1988.

[13] B. M. A. Rahman and J. B. Davies, "Finite element solution of integrated optical waveguides," *J. Lightw. Technol.*, vol. 2, no. 5, pp. 682–688, Oct. 1984.

[14] K. Hayata, M. Koshiba, and M. Suzuki, "Lateral mode analysis of buried heterostructure diode lasers by the finite-element method," *IEEE J. Quantum Electron.*, vol. QE-22, no. 6, pp. 781–788, Jun. 1986.

[15] A. D. McAulay, "Variational finite-element solution for dissipative waveguides and transportation application," *IEEE Trans. Microw. Theory Techn.*, vol. MTT-25, no. 5, pp. 382–392, May 1977.

[16] K. Hayata, K. Miura, and M. Koshiba, "Finite element formulation for lossy waveguides," *IEEE Trans. Microw. Theory Techn.*, vol. 36, no. 2, pp. 268–276, Feb. 1988.

[17] S. R. Cvetkovic and J. B. Davies, "Self-adjoint vector variational formulation for lossy anisotropic dielectric waveguide," *IEEE Trans. Microw. Theory Techn.*, vol. MTT-34, no. 1, pp. 129–134, Jan. 1986.
[18] S. S. A. Obayya, B. M. A. Rahman, and H. A. El-Mikati, "New full-vectorial numerically efficient propagation algorithm based on the finite element method," *J. Lightw. Technol.*, vol. 18, no. 3, pp. 409–415, Mar. 2000.
[19] M. Rajarajan *et al.,* "Review of finite-element characterization of photonic devices," *J. Mod. Opt.*, vol. 50, no. 12, pp. 1835–1848, 2003.